Correspondence to:
M. T. O'Connor,
mtoconnor12@gmail.com

Active Layer Groundwater Flow: The Interrelated Effects of Stratigraphy, Thaw, and Topography

Michael T. O'Connor[1], **M. Bayani Cardenas[1]**, **Bethany T. Neilson[2]**,
Kindra D. Nicholaides[1], and **George W. Kling[3]**

[1]Department of Geological Sciences, The University of Texas at Austin, Austin, TX, USA, [2]Civil and Environmental Engineering, Utah Water Research Laboratory, Utah State University, Logan, UT, USA, [3]Deparment of Ecology and Evolutionary Biology, University of Michigan, Ann Arbor, MI, USA

Abstract The external drivers and internal controls of groundwater flow in the thawed "active layer" above permafrost are poorly constrained because they are dynamic and spatially variable. Understanding these controls is critical because groundwater can supply solutes such as dissolved organic matter to surface water bodies. We calculated steady-state three-dimensional suprapermafrost groundwater flow through the active layer using measurements of aquifer geometry, saturated thickness, and hydraulic properties collected from two major landscape types over time within a first-order Arctic watershed. The depth position and thickness of the saturated zone is the dominant control of groundwater flow variability between sites and during different times of year. The effect of water table depth on groundwater flow dwarfs the effect of thaw depth. In landscapes with low land-surface slopes (2–4%), a combination of higher water tables and thicker, permeable peat deposits cause relatively constant groundwater flows between the early and late thawed seasons. Landscapes with larger land-surface slopes (4–10%) have both deeper water tables and thinner peat deposits; here the commonly observed permeability decrease with depth is more pronounced than in flatter areas, and groundwater flows decrease significantly between early and late summer as the water table drops. Groundwater flows are also affected by microtopographic features that retain groundwater that could otherwise be released as the active layer deepens. The dominant sources of groundwater, and thus dissolved organic matter, are likely wet, flatter regions with thick organic layers. This finding informs fluid flow and solute transport dynamics for the present and future Arctic.

Plain Language Summary Groundwater flow in permafrost watersheds is potentially a key component of global carbon budgets because permafrost soil stores vast amounts of carbon that could be mobilized due to a warming climate and the corresponding increase in soil thaw. In addition to carrying carbon, groundwater can supply important nutrients and solutes to surface waters. However, we do not yet understand the factors that control groundwater flow in soils above permafrost because saturation changes rapidly and continuously, and soil hydraulic properties are largely unknown. We created measurement-informed calculations of groundwater flow from areas of permafrost with different characteristics and found that soil types, which vary based on the slope of the land surface, are the most important control. Near-surface soils were identical in hillslopes and valleys, whereas deeper soils in hillslopes allowed for less groundwater flow than in valleys. In early summer, when only the near-surface soils were thawed, groundwater flows in the hillslopes and valley were similar. In late summer, when the deeper soil was thawed, groundwater flow in the valley remained high, but flow in the hillslope was negligible. Our observations also showed that small mounds on the land surface caused groundwater to be trapped behind underground ice dams.

1. Introduction

Arctic warming is accelerating permafrost thaw which will allow for unknown amounts of groundwater to dissolve and mobilize soil constituents through groundwater flow (Frey & McClelland, 2009; Walvoord & Striegl, 2007). Given the vast volume of carbon in Arctic soils, its transport by groundwater could substantially impact the global carbon cycle (e.g., Hobbie & Kling, 2014; Ping et al., 2008). Groundwater flow occurs in permafrost regions through suprapermafrost, intrapermafrost, or subpermafrost aquifers (Woo, 2012). However, the understanding of groundwater flow in areas of continuous permafrost has critical gaps. In particular for suprapermafrost aquifers, aquifer geometry and hydraulic properties vary in an often-ignored but

important way: The water table and the ice table both migrate vertically into soils of vastly differing permeability and porosity.

Groundwater flow in any saturated porous media is described by Darcy's Law:

$$Q = KA\nabla h, \tag{1}$$

where Q is volumetric groundwater flow (L^3/T); it is controlled by ∇h, the hydraulic head gradient (L/L), K, the hydraulic conductivity (L/T), and A, the aquifer cross sectional area (L^2), which is determined by the saturated thickness b (L) and some unit width w (L). Fluctuations in the water table, driven by precipitation and drainage, change both the thickness and the overall hydraulic conductivity of a suprapermafrost aquifer by incorporating (in the case of a rising water table) or excluding (in the case of a falling water table) overlying soil layers with potentially different hydraulic properties than underlying soils (Figure 1). Commonly, these water table fluctuations are negligible when compared to the entire thickness of an aquifer and are therefore ignored in groundwater flow calculations through the application of the Boussinesq equation for unconfined aquifers (Cardenas, 2010). However, suprapermafrost aquifers in areas with continuous permafrost are typically quite thin: Active layer thicknesses, the extent of the zone that thaws annually, in the continuous permafrost found on the North Slope of Alaska and the Yukon Territory in Canada range between approximately 40 and 80 cm (Hinkel & Nelson, 2003; Nelson et al., 1999; Quinton et al., 2005; Smith et al., 2009). Furthermore, previous work showed that saturated K within Arctic and boreal peatlands can be 2 orders of magnitude higher at the surface than at 30-cm depth (Ebel et al., 2019; Hinzman et al., 1991; Quinton et al., 2000). Decimeter-scale water table fluctuations within suprapermafrost aquifers can therefore represent substantial changes to both b and K and, by extension, Q and should not be ignored or approximated. From here on, we exclusively refer to and interchangeably use suprapermafrost and active layer aquifer or groundwater when we use the terms "aquifer" and "groundwater."

Ice table fluctuations are an additional factor that potentially drive substantial changes to aquifer b, K, and Q. Unlike in typical aquifers with no ice, where the bottom boundary is defined by lithology, the bottom boundary of a permafrost aquifer is defined by a time-variable and moving frozen surface. The temporal migration of that surface, both within a season and between seasons, exposes new and deeper soil layers with hydraulic properties that can differ from those in the soil above it and thus affects the hydraulic properties of the entire permafrost aquifer. Few studies consider the impact that ice table migration could have on soil hydraulic properties and subsequent groundwater flows, which has led to wide uncertainty in the prediction of future groundwater flows in the Arctic (Walvoord & Kurylyk, 2016).

It is unclear what effect the migration of the water and ice tables will have on b, K, and Q. As the summer season progresses, the saturated zone within the active layer tends to thicken as the thaw depth increases, which would increase groundwater flows. However, the saturated zone can deepen into less permeable soil, which could decrease flows. The interplay between these factors can be quantified through hydraulic transmissivity (T; L^2/T), which is the product of K and b; however, active layer T, and its variation in time and space, is currently uncharacterized because few measurements of K and b have been made in continuous permafrost environments. Previous studies have measured depth-dependent relationships for saturated and unsaturated K (Hinzman et al., 1991; Quinton et al., 2000), but the lateral spatial variability of these parameters across different landscape types is poorly quantified. Additionally, while previous work has characterized both temporal variability and microtopographic variability in b in a permafrost environment (Pomeroy et al., 2007; Quinton et al., 2000, 2005), how b varies across and within different landscape types such as hillslopes or valley bottoms remains unknown. Because we lack knowledge on how K and b vary in time and space, the interplay of K and b in affecting T and, ultimately, groundwater flows is also poorly understood.

There have been many previous interrogations of groundwater flows in peat-dominated, continuous permafrost environments using both field methods and numerical methods. However, these studies could not investigate how the impact of K and b interactions affects groundwater flows. For example, field-based studies of active layer groundwater flows have employed baseflow separation (e.g., McNamara et al., 1997; Stieglitz et al., 2003), geochemical methods (e.g., Blaen, 2013; McNamara et al., 1997; Walvoord & Striegl, 2007), and water balance calculations (e.g., Roulet et al., 1993). While these methods can determine integrated groundwater contributions to streamflow, they do not consider the subsurface mechanisms that
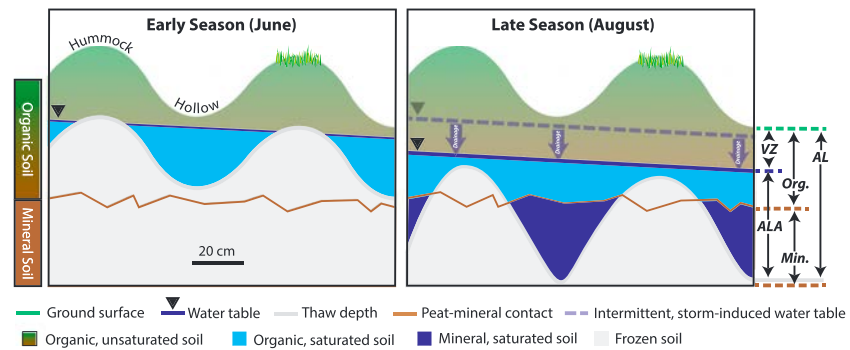
Figure 1. Conceptualized cross section of groundwater flow in the active layer in Early Season (left) and Late Season (right). The panels highlight the potential spatial variability of the active layer saturated zone (ALA), both in position and in thickness, as well as the temporal variability in both those factors. Although it is not depicted, flow comes into and out of the plane illustrated as the system is three-dimensional; such flow connects seemingly isolated pools observed in the Early Season (June) panel. Note that in this conceptual model, the water table is shown as planar, rather than as a subdued replica of topography, as is often the case in groundwater hydrology illustrations. The observations did not support a water table reflecting topography, and studies conducted in similar settings also observe a planar water table despite undulating topography (e.g., Figure 2, Quinton et al., 2000).

drive groundwater contributions. Thus, indirect, field-based groundwater flow studies are unable to predict how groundwater flows may change as K and b change; they can only predict the integrated, net effect of those changes. Studies that rely on process-based numerical models to calculate groundwater flows (e.g., Atchley et al., 2015; Frampton et al., 2011; Schuh et al., 2017) inherently consider the effects of changes to K and b, as well as any other groundwater flow parameter. However, these studies are rarely informed by field observations of the water table and the ice table, and they often parameterize K based on small sample sizes (Hinzman et al., 1991; Quinton et al., 2008).

Here we determine how changes in summer seasonal thaw and water table depth impact transmissivity and groundwater flow. We investigated this through high-density grids of direct field observations that were used as direct inputs to groundwater flow model calculations of fluxes. Additional calculations were completed using the same models to analyze sensitivity to water table depth. The observational approach was designed to determine well-constrained estimates of transmissivity and flow through the direct measurement of saturated thickness, hydraulic conductivity, and hydraulic gradient. This provided insight regarding transmissivity and flow changes as the season progressed, across different topographic settings, and within the same topographic setting. Sensitivity analysis was designed and conducted to determine the dependence of transmissivity and flow estimates, if any, to minor, hypothetical changes in the water table location. The findings from this study highlight the impact of highly dynamic active layer response on groundwater flows. The study provides foundational knowledge regarding suprapermafrost aquifers, which could ultimately help predict their state under further warming.

2. Study Site and Experimental Design

To test how groundwater flows in the active layer vary across space and through time, we established regularly spaced, high-density measurement grids within Imnavait Creek Watershed, a 2.2-km² first-order watershed (McNamara et al., 1997; Merck et al., 2012) underlain by hundreds of meters of continuous permafrost (Osterkamp & Payne, 1981). The watershed is a representative study site for understanding hydrologic behavior in the Arctic, as it exhibits the geology, climate, and ecology typical of a headwater catchment in the Arctic Foothills (Walker & Walker, 1996). The Arctic Foothills is one of only two United States Geological Survey-designated physiographic regions (Wahrhaftig, 1965) and United States Environmental Protection Agency-designated ecoregions (Omernik & Griffith, 2014) found in Alaska's North Slope, and thus, it represents a large area key to understanding Arctic groundwater flows. The Arctic Foothills is defined largely by topography, containing moderate to steep rolling hills carved by six distinct glaciations in the late Pleistocene (Detterman et al., 1958; Hamilton, 1982). The Arctic Foothills is bounded to the south by the Brooks Range and to the north by the much flatter Arctic Coastal Plain, and the Coastal Plain is bounded to the north by the Arctic Ocean (Figure 2, inset). Summer air temperatures range between 6
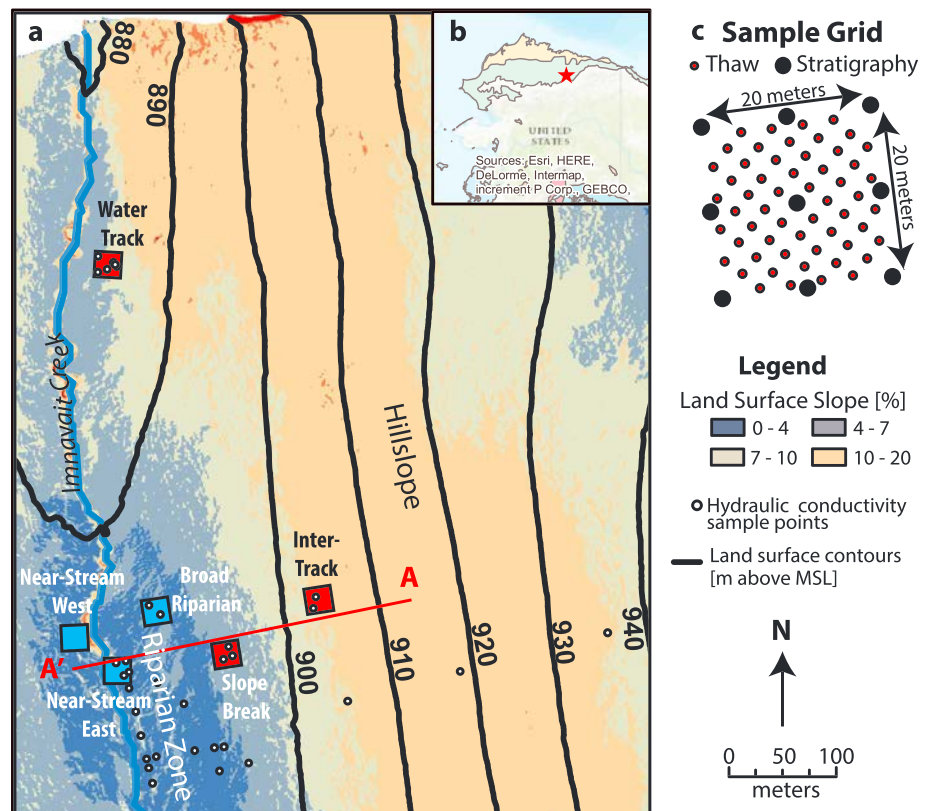
Figure 2. Map of field site. (clockwise from top right) Locations of the six sample grids within Imnavait Creek Watershed, underlain by topographic slope (a); map of Alaska, showing location of Imnavait Creek (red star) and the two EPA Ecoregions of the North Slope, the Foothills (green), and Coastal Plain (yellow) (b); and locations of individual sample points within each grid (c). The riparian zone is indicated by the darkest blue section of the map; the hillslope is represented by all other colors.

and 18 °C, and the watershed receives 35 cm of precipitation a year on average, with 60% of that occurring as summer rain (McNamara et al., 1997). The Late Season active layer thicknesses measured at Imnavait Creek are approximately 50 cm, but the measurement range is substantial (Nelson et al., 1999).

Walker and Walker (1996) identified two dominant landscape zones, the hillslope and riparian area, which together comprise 90% of Imnavait Creek Watershed. The remaining 10% is largely defined as bare ground and dwarf heath vegetation on ridge tops, which are typically hydrologically disconnected from the rest of the watershed (Stieglitz et al., 2003). We established multiple observation grids in each zone to capture the spatial variability between and within the zones (Figure 2). These landscape zones are topographically distinct: Hillslopes have broad and linear 4% to 20% slopes leading to the basin spine, and riparian zone slopes are shallower than 4%. The hillslope zone is asymmetric: The west-facing hillslope is broad, extending over 600 m from the creek to the watershed divide, while the east-facing hillslope has about one sixth that reach. The hillslope and riparian zones differ substantially in active layer thicknesses, vegetation composition, and soil stratigraphy (Stieglitz et al., 2003; Walker & Everett, 1991; Walker & Walker, 1996).

Our observation grids include the dominant microtopographic features within each landscape zone (Tables 1 and 2). Water tracks represent a dominant hillslope zone microtopographic feature (Walker & Walker, 1996). Water tracks are zero-order geomorphic drainage features that can funnel substantial water flows from the hillslope (McNamara et al., 1999). These linear drainage features, spaced somewhat regularly in intervals of tens of meters, develop in subtle topographic lows within the landscape (McNamara et al., 1997; Voytek et al., 2016). They are unique to tundra environments in that while they resemble streams in their morphology and retain moisture for substantially longer periods than the surrounding intertrack areas (Rushlow & Godsey, 2017), they rarely exhibit surface flow because shallow permafrost prevents the erosive

Table 1
Description of Study Grids Within the Imnavait Creek Watershed

Grid name	Landscape zone	Land surface slope (%)	Average microtopography peak-to-trough height (cm)	Notable features
Inter-Track	Hillslope	10.6	7.5	No anomalous land surface slope or microtopography characteristics
Water Track	Hillslope	6.7	6.5	Grid bounded on the south edge by a continually wet but rarely flowing water track
Slope Break	Hillslope	5.6	7.1	Grid reflects hillslope topography; however, it sits just above the abrupt transition between Hillslope and Riparian
Broad Riparian	Riparian	3.9	5.1	No anomalous land surface slope or microtopography characteristics
Near-Stream East	Riparian	3.0	7.3	Microtopography is more present; grid bisects the stream on its western face
Near-Stream West	Riparian	3.2	7.0	Water track on southern border; grid bisects stream on its eastern face

processes necessary to carve out a stream channel (McNamara et al., 1999). They therefore accumulate lateral hillslope groundwater flow and then route that water downslope via both surface and shallow groundwater flow. These features are most easily distinguished by a change in vegetation from tussocks that dominate the surrounding hillslope to willows in the water tracks. Our study contained two hillslope zone grids; one included a water track (the "Water Track grid"), and one did not (the "Inter-Track grid").

Water tracks are not observed in the riparian zone grids, as the concentrated flow derived from these confined linear features diffuses broadly when the land surface slopes decrease (McNamara et al., 1997). Rather, the dominant microtopographic features in the riparian zone are "hummocks," small mounds that develop due to frost-heave processes, and subsequent "hollows," the depressions found in between hummocks (Quinton et al., 2000). Hummocks vary in size but serve a similar function as water tracks in that they drive spatial variability in saturation within the grids by concentrating water in local depressions. Our three

Table 2
Summary of Means (μ) and Standard Deviations (σ) of Measurements and Calculations From Each Measurement Grid

		Inter-Track		Water Track		Slope Break		Broad Riparian		Near-Stream East		Near-Stream West	
		μ	σ	μ	σ	μ	σ	μ	σ	μ	σ	μ	σ
Land surface slope (%)		10.6	1.6	6.7	1.2	5.6	1.1	3.9	1.1	3.0	1.3	3.2	1.3
Microtopography peak-to-trough height (cm)		7.5	1.3	6.5	0.3	7.1	0.0	5.1	0.5	7.3	2.0	7.1	1.8
Depth to catotelm (cm)		12.0	6.4	23.7	10.6	18.0	8.1	18.6	7.7	18.6	7.7	12.7	10.7
Depth to loess (cm)		21.4	3.7	20.9	7.9	24.7	3.8	NA	NA	NA	NA	34.9	10.4
Water table depth (cm)	June	11.4	3.3	7.8	3.3	9.3	6.2	8.4	6.0	8.6	4.6	10.0	5.7
	August	21.0	3.6	20.9	7.9	18.0	8.6	8.4	9.2	15.7	13.4	21.4	10.0
Thaw depth (cm)	June	11.9	3.7	10.3	3.9	14.7	6.8	15.8	4.4	15.2	4.7	16.7	6.1
	August	43.7	8.1	74.0	18.4	55.7	11.5	46.9	8.8	51.9	11.8	53.6	9.6
Saturated thickness (cm)	June	0.5	1.8	2.5	3.9	5.7	6.0	7.4	5.2	6.5	7.6	6.3	6.4
	August	22.9	8.7	52.0	19.5	38.6	13.3	39.2	8.4	36.2	22.3	31.7	15.3
Transmissivity (m^2/day)	June	0.45	1.59	2.23	4.23	1.02	2.62	2.92	4.80	1.33	3.18	0.97	2.36
	August	0.11	0.85	0.05	0.31	0.13	0.59	2.99	4.28	2.73	4.53	0.76	2.24
Hydraulic gradient (%)	June	10.7	1.8	6.9	1.1	5.4	1.4	4.0	0.6	2.7	1.1	3.2	0.9
	August	10.2	1.1	6.7	2.2	5.7	1.1	4.2	1.0	2.8	0.6	4.4	2.1
Groundwater Flow (m^3/day)	June	0.54	0.09	1.83	0.33	0.69	0.17	1.50	0.24	0.46	0.20	0.34	0.10
	August	0.17	0.05	0.04	0.02	0.10	0.02	1.63	0.37	0.97	0.22	0.40	0.19

Note. The grid locations are depicted in Figure 2. NA = not applicable.

riparian zone grids contained hummocks of varying sizes (see "average microtopography peak-to-trough height" in Table 1), allowing us to determine their potential effects on b, K, ∇h, T, and groundwater flow.

We set one grid on either side of the creek within the asymmetric riparian zone (six times more area on the western face). These opposing grids have comparable land surface slopes and size scales of microtopography and are located at the same distance upstream from the main weir. This allows for a comparison of hydrologic properties and flows from contributing areas of substantially different sizes.

3. Methods

To understand the factors controlling groundwater flow within the active layer aquifers, we collected original field measurements in grids of high spatial resolution at two points in time within the summer of 2016. We employed standard statistical methods to determine spatial and temporal differences and patterns within the data. We then used these data as boundary, geometry, and parameter constraints for direct, observation-based 3-D groundwater flow calculations and sensitivity analyses to determine the impact of a fluctuating water table on groundwater flow.

3.1. Field Measurements of Ground Surface, Thaw Depth, Water Table, and Soil Hydraulic Properties

Thaw depth and water table elevation data were collected at 61 evenly spaced measurement points within each grid (Figure 2). Thaw depth was measured using a graduated 1.2-m-long metal rod that was driven into the ground until refusal. Three measurements were taken near each point and averaged. Water levels were measured within 0.5″ and 0.75″ diameter PVC piezometers installed at each point, screened over the bottom 20 cm, and sealed at the bottom with epoxy. These measurements were taken during the early summer (9–15 June) and late summer (7–10 August) of 2016.

Stratigraphic data (layer thickness and depth) were collected within measurement grids during late summer, at a sparser spatial resolution to minimize local disturbance. Measurements were made at 9 equally spaced points within the original 61 points (see Figure 2c). We measured the depths to the contacts between the organic and mineral soil types from a core withdrawn using a 2″ diameter, 24″ long soil corer (AMS, American Falls, Idaho), which was driven into the ground until refusal then removed.

Saturated K was measured in the field at various depths within the six sampling grids using three different methods. Multiple methods were necessary to determine K across the depths and locations of the study site due to the requirements for each method. In locations where we were able to isolate a saturated depth segment of soil, we determined K in situ with slug tests as described by Surridge et al. (2005). We performed 26 total slug tests at depths ranging from 11 to 85 cm. To perform the test, a 2″ diameter drive-point piezometer (composed of a 20-cm screen below 1 m of PVC casing and sealed with epoxy) was driven into the ground to the desired depth of the measurement. Water displacement during a slug test was measured with a fast-response pressure transducer (Aqua Troll 700, In Situ, Fort Collins, CO) placed at the bottom of the well. K was calculated by analyzing the water level recovery recorded by the pressure transducer following the theory of Bouwer and Rice (1976). The slug tests lasted several seconds to a few minutes. Water level logging rates were set at 0.25 s. The K values from the slug test represent the effective horizontal K across the saturated depth segment.

Given that in situ slug tests must be performed within a fully saturated aquifer depth segment, the full range of slopes and depths necessary for this investigation was not covered by in situ tests because there were many locations in which a saturated depth interval was unavailable. To complete the sample set, soil cores from unsaturated locations were extracted and analyzed in the lab using two methods. For intact 5-cm-diameter cores, saturated K was measured using a constant-head test implemented with a KSAT Benchtop Hydraulic Conductivity instrument (UMS Corp., Berlin, Germany). Our cores provided soil K over a 5-cm depth segment, and soil depths ranged from 0 to 50 cm.

For mineral soil samples, the retrieval of an undisturbed, intact 5-cm core was impossible in the field due to the depth of the sample, and the aquifer response to the slug test was too slow to be measured. We therefore used an empirical method based on grain size to estimate K in these samples. Eleven samples of mineral soil were collected from an AMS Soil Corer for grain size analysis using a wet sieve for particles above 74 µm (No. 200 sieve) and laser particle refraction for particles smaller than 74 µm (Liu et al., 2005). The d_{50} (50th

percentile or median) of the grain sizes was then used to predict K via the Carman-Kozeny model (Carman, 1956).

3.2. Statistical Analysis and Grouping of Soil Hydraulic Conductivity Distributions

Statistical patterns within K measurements were identified by first grouping the measurements with respect to soil type and then grouping them by depth. We assigned soil types for each of the soil core samples visually, and we assigned the soil types for all in situ slug test samples based on the nearest extracted soil core (because we obviously could not directly observe what soil the screened interval spanned). The soil type was classified either as acrotelm, catotelm, or mineral soil. We used a two-sample Mann-Whitney U Test to determine if the K values of each soil group were different to a 5% significance level ($p = 0.05$). Within each soil type, we grouped our measurements into 5-cm depth segments and performed a Kruskal-Wallis one-way analysis of variance across all depth segments to determine if there were statistically significant decreases in K with depth. We lastly performed regressions of K with depth to build a functional relationship to predict K with depth.

3.3. Analysis of the Field Measurements and Their Spatial and Temporal Differences

The field measurement grids were categorized by landscape zone, and intragrid measurements were identified by their microtopographic position (i.e., the relative vertical position of each point with respect to the average land surface elevation). To determine the landscape zone, we calculated the land surface slope based on a 20-cm spatial resolution digital elevation model (DEM) of the watershed collected in April 2015 (Fairbanks Fodar, Fairbanks, Alaska). A slope threshold of 4% separated the hillslope and riparian landscape zones (Figure 2); this resulted in three of the six sample grids falling in the hillslope zone and three falling in the riparian zone.

The microtopographic position of each sample point was determined by fitting a linear, first-order polynomial surface to the land surface elevation measurements collected at each of the 61 grid points. This surface represented the average land surface slope of the entire grid. We then identified individual measurement points as either a local elevation high or a low based on the difference between the actual measured elevation and the elevation of each point based on the calculated average land surface slope. A positive difference between actual and average elevations denoted a local high, and a negative difference denoted a local low.

The average ∇h for each grid was determined by fitting a linear, first-order polynomial surface to the measured water table elevations. The slope of that surface represented the average ∇h within each plot.

Using the above criteria, we compared how active layer thickness, $\nabla h, b, K, T$, and estimated groundwater flows varied across landscape zones, microtopography, and season. Comparisons were performed using nonparametric statistical tests in which each measurement was grouped into populations based on landscape zone, microtopographic size, or season. The uniqueness of these populations was determined using a two-sample Mann-Whitney U Test when comparing two populations and a Kruskal-Wallis one-way analysis of variance when comparing more than two populations. Any p value below 0.05 determined from these tests is considered statistically significant.

3.4. Calculation of Transmissivity

Transmissivity (T) describes the integrated lateral K of an aquifer over some vertical interval or thickness b. When K is depth dependent, the equation for T is

$$T|_{z_1}^{z_2} = \int_{z_1}^{z_2} K(z) \mathrm{d}z, \tag{2}$$

where z_1 and z_2 are the bottom and top of the aquifer saturated zone (or any two arbitrary vertical points), respectively (L). We applied $K(z)$ relationships established from measurements (described above) along with the depths of the water table (z_2) and ice table (z_1) to analytically compute T at every measurement point on the landscape. We then compared the computed T at these measurement points between landscape zones and microtopographic position based on the same statistical tests described in section 3.3.

3.5. Calculation of Groundwater Flow Using 3-D, Steady-State Groundwater Flow Models
3.5.1. Model Development

Two sets of 3-D, steady-state saturated groundwater flow models were constructed: One set was informed fully by observation, and one set was only partially informed by observation because hypothetical water
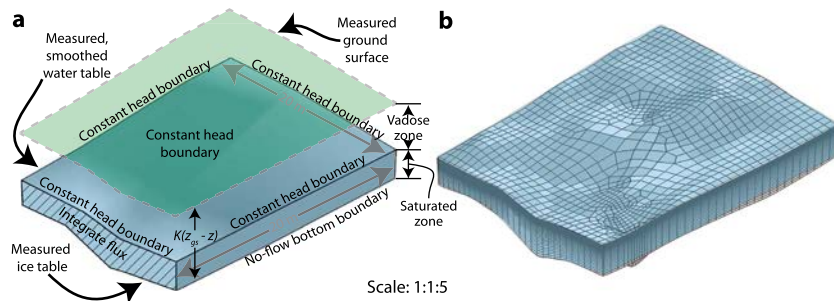
Figure 3. Schematic of 3-D saturated groundwater flow models constructed to calculate groundwater flows. (a) Model domain, boundary conditions, and hydraulic conductivity parameterization. The green surface represents the measured ground surface elevation, which provided the reference for calculating depth-dependent K. The blue box represents the saturated model domain, bounded above by a Lowess Regression-smoothed water table and below by the measured ice table of each grid. The water table defines the constant head boundary on all sides and the top of the domain; the bottom boundary condition is no flow. Assignment of K and boundary conditions is consistent throughout all the models in this study; however, the position of the ground surface, water table, and ice table vary due to grid location and study time. The "Early Season" model series employed the June measured surfaces; the "Late Season" model series employed the August measured surfaces; the "Variable Water Table" sensitivity analysis employed the August ground surface and ice table and shifted the August water table in 5-cm increments between those two boundaries. (b) Unstructured mesh illustration used in the groundwater flow models. We employed 3-D quadrilateral elements whose z-dimension thickness increased in a geometric sequence from the water table to the ice table in order to capture the steep depth-dependent K decay observed at shallow depths.

table locations were imposed (Figure 3). The observational set was designed to estimate in situ groundwater flows, and the partially observational set was conducted for sensitivity analysis with regard to water table depth. As stated above, the groundwater flow equation can be solved given prescribed hydraulic conductivity, hydraulic head distribution, and cross-sectional area at a fine spatial resolution and results in estimates of groundwater flow through each grid. Conventional applications of groundwater models require parameter tuning to correctly calculate the position of the water table or soil hydraulic conductivity in unknown locations (Wang & Anderson, 1995); however, in our models, both the water table position and the hydraulic conductivity are well-defined at a sufficiently fine spatial resolution and do not require adjustment. We can therefore directly apply these measurements to the model to calculate groundwater flow.

The geometry, boundary conditions, and hydraulic properties for each calculation were informed by the measurements described previously. The equation for steady-state 3-D saturated groundwater flow in an aquifer with locally isotropic but systematically heterogeneous K and without sinks or sources is

$$\nabla \cdot -K(z)\nabla h = 0. \tag{3}$$

While the specific values of hydraulic properties and boundary conditions for the model are not identical between grids, the method used to apply them to each grid is consistent. The hydraulic heads at the top boundary and all side boundaries were fixed at the elevation of the measured water table:

$$h_{\text{top,sides}} = z_{\text{wt}}, \tag{4}$$

where z_{wt} is the observed water table elevation at all grid measurement points. The bottom boundary in each model, that is, the thaw depth, was assigned as a no-flow boundary:

$$n \cdot -K(z)\nabla h = 0, \tag{5}$$

where n is the vector normal to that bottom boundary. K was defined using the depth function described in section 3.1 (Figure 4). The groundwater flow equation was numerically solved using quadrilateral mesh elements that were narrowest at the top of the domain (the water table) and grew in a geometric sequence to the bottom (the ice table; Figure 3). This meshing framework was used to represent the rapid depth-dependent changes in K observed near the ground surface, at the top of the model domain. The calculation was performed using the finite-element modeling software COMSOL Multiphysics.
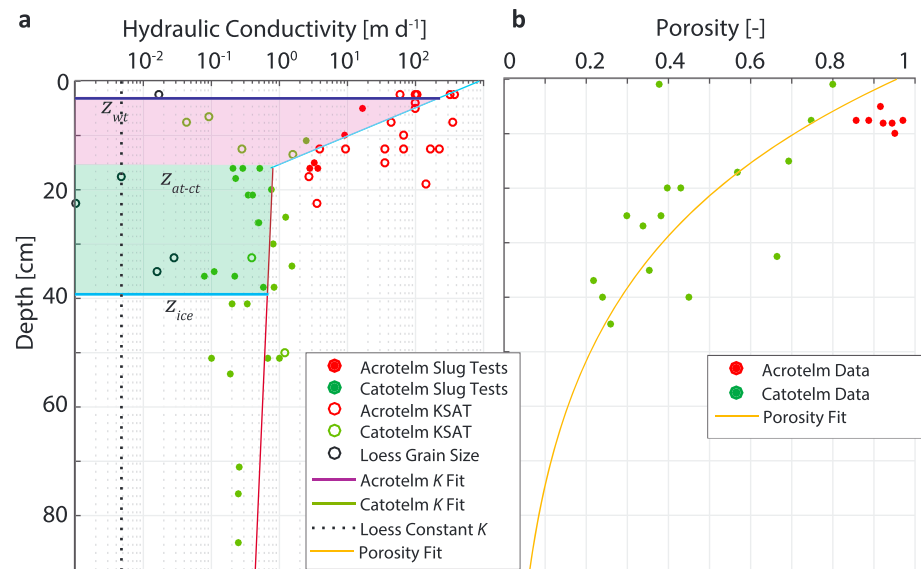
Figure 4. Depth distribution of measured (a) K and (b) porosity of all samples. The solid lines are fitted curves based on soil type (a) or across all soil types (b). All mineral soil samples were analyzed via the grain size method (open black circles); among catotelm and acrotelm samples, open circles denote measurements taken in the laboratory with a constant-head test apparatus, and filled circles represent measurements taken in situ via slug tests. The purple and green shaded boxes graphically represent the T of the acrotelm and catotelm segment of the profile.

For all calculations, we used a Lowess Regression to interpolate a smooth surface based on our measured water table elevations (Trexler & Travis, 1993). This step was necessary to smooth out peaks and valleys within the water table measurements that caused the groundwater flow field to develop large, anomalous, and nonphysical groundwater sink and source locations. Such locations are likely the result of easily deformable ground affecting the accuracy of land surface survey measurements. This happened rarely; the goodness-of-fit coefficient for the Lowess Regressions exceeded 0.9 for all models.

We determined the total groundwater flow out of the domain (Q_{out}) by aerially integrating the groundwater flow through the downslope boundary:

$$\int [n \cdot -K\nabla H] = Q_{out}, \tag{6}$$

where n is the vector normal to the downslope boundary; this face is represented in Figure 3.

3.5.2. Observation-Informed Calculations: Early and Late Seasons

A groundwater flow calculation was performed for each of the six measured grids at each of the two times that the measurements were taken; thus, a unique 3-D model domain was constructed for each case. This led to the construction of a total of 12 3-D models. The water table measurements (i.e., the top hydraulic boundary condition) and ice table measurements (i.e., the bottom of the domain) collected within the six grids in June were used to develop the "Early Season" modeling scenario, and those measurements collected within the six grids in August were used to develop the "Late Season" modeling scenario. We used the same hydraulic conductivity profiles in both the Early Season and Late Season scenarios.

3.5.3. Variable Water Table Sensitivity Analysis

In addition to calculating groundwater flows given observed water table and ice table conditions, we also performed a sensitivity analysis for determining how transmissivity and groundwater flows are impacted by small shifts in the water table depth given the same ice table depth. To do this, we altered the observed Late Season 3-D model domains by shifting the measured August water table upward until it was at the ground surface and then progressively downward in 5-cm increments. The incremental contribution of groundwater flow for each 5-cm depth segment was then computed by taking the difference in groundwater flow between consecutive model runs. For example, the groundwater contribution of the depth segment between 5 and 10 cm was determined as the difference between the groundwater flow computed

with a 5-cm deep water table and with a 10-cm deep water table. While the prescribed water table elevations are not directly informed by measurements, published observations (e.g., Schramm et al., 2007, figure 9) show that the water table within the active layer does range from fully saturated to fully drained; thus, these imposed scenarios represent realistic, although not necessarily observed, conditions.

The Variable Water Table sensitivity analysis shifted the top boundary of the 3-D models (the water table) while keeping the bottom boundary (the ice table) fixed at the measured Late Season depth. The ice table is near or at its deepest point in August; therefore, the total groundwater flows calculated from this sensitivity analysis are reflective of a thawed depth that is larger than average and could result in flows that are biased high. However, the purpose and design of this sensitivity analysis is not to consider total groundwater flows but rather to consider the incremental groundwater flow contribution of each 5-cm soil layer inundated by a shifting water table. Thus, the assignment of a deep and constant ice table should not substantially affect the findings of this analysis.

4. Results

Our findings showed that spatial variability in active layer stratigraphy and b and temporal variability in saturated zone position based on landscape zone cause important differences in T and groundwater flow. Particularly, the thick soils in the low-gradient riparian zone can transmit groundwater for the duration of the summer, while the thinner soil hillslope only briefly provides flow.

4.1. Spatial Variability in Hydraulic Conductivity

Three distinct soil layers were found consistently across all grids: acrotelm (living or recently dead but not decomposing peat; Holden & Burt, 2003), catotelm (decomposing and compressed peats; Morris et al., 2011), and loess mineral soil (wind-blown, fine-grained sediments; Walker & Everett, 1991; Figure 4). These layers have been identified across the Arctic Foothills in previous work (Walker et al., 2003). The K of these materials differed significantly both between and within soil types. The K of the acrotelm and catotelm deposits decayed significantly with depth, whereas the K in loess did not. Broadly speaking, the most surficial acrotelm is very permeable because its high porosity creates little to no resistance to flow (Quinton et al., 2008). K measured in these soils can exceed 800 m/day (equivalent to marble-sized gravel). However, peat soils compact readily as they degrade (van Asselen et al., 2009), and thus, the K also decreases with age of the organic layer and correspondingly with depth (Beckwith et al., 2003). We observed two distinct patterns of decreases in K with depth in the acrotelm and catotelm. The exponential decrease (or decay) of acrotelm K was most substantial, dropping 3 orders of magnitude from the surface to the base of the acrotelm layer, and porosity decreased 30% in that same interval (Figure 4). The decrease in K observed in the catotelm was less prominent, dropping approximately 60% between the top and the base of the catotelm; however, the reduction in porosity continued, decreasing approximately 50% over the same depths (Figure 4). The rate of K decrease with depth in the catotelm is similar to rates of decrease observed in previous work in both Arctic and temperate zone locations (Beckwith et al., 2003; Quinton et al., 2008). We observed no differences in K decrease with depth across different landscape zones or microtopographic locations.

The K of the loess soils changes little with depth and is consistently very low. The average K of such deposits was 0.004 m/day (Figure 4), 2 orders of magnitude lower than the deepest catotelm samples. We did not observe significant ranges in loess soil K across grids; however, loess K sample size was low. The K values we measured fall within typical ranges for loess soils (Freeze & Cherry, 1979).

We conducted a series of regressions to determine a piecewise relationship between K and depth:

$$K(z) = \begin{cases} 10^{-19.17z+2.937}, & z<z_a \\ 10^{-0.35z}, & z_a<z<z_m , \\ 10^{-2.39}, & z>z_m \end{cases} \qquad (7)$$

where z is the depth of the soil (m), z_a is the depth to the inflection point in the K-depth curve (established to be 0.15 m; Figure 4), z_m is the depth to the catotelm base (if observed; m), and K is in meters per day. z_a approximately represents the contact between acrotelm and catotelm soils, although as described below, the contact depths between acrotelm and catotelm soils change with landscape type and
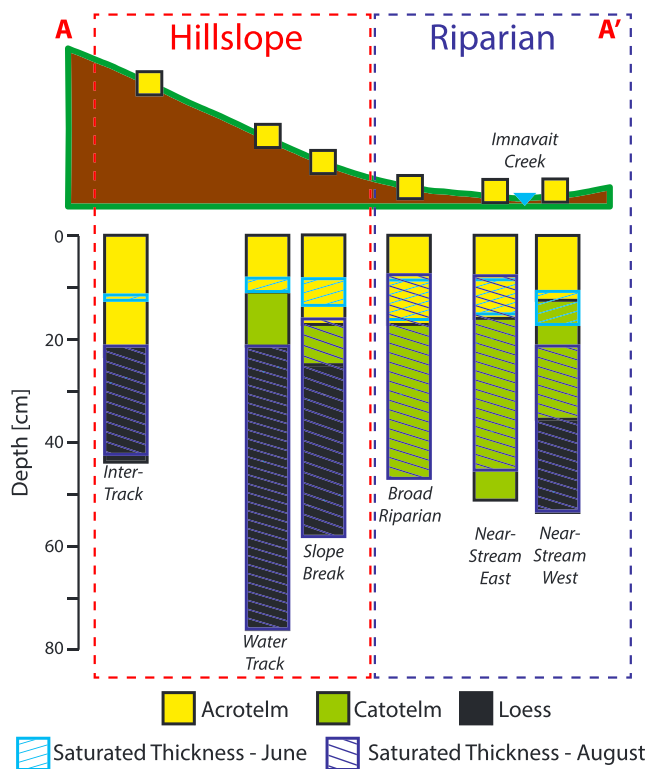
Figure 5. Average thickness of the acrotelm, catotelm, and loess (when present) within each of the six sampling grids, with June and August saturated thicknesses superimposed on the columns. The bottom boundary of each saturated thickness is defined by the ice table at the time of measurement. Grids are represented by yellow squares on the cross section above; the cross section A-A′ can be found on Figure 2. The water track grid, which does not fall within the A-A′ cross section, is included here at its approximate position downslope from its nearest ridge.

microtopographic position. When the catotelm base was not observed, equation (7) is limited to only the upper two sections.

4.2. Hydrostratigraphic Variation

Given the variation in K observed both between and within soil types, an accurate determination of groundwater flows in this landscape requires knowing where each soil contact lies, especially in relation to the water table. The measurements show that the thickness and depth of the soil layers differ predictably both between and within landscape zones.

The total peat thickness (acrotelm plus catotelm) increased across grids as the grid position migrated downslope. The measured total peat thickness in the low-slope riparian sites (48 ± 18 cm) was significantly larger than in the two steepest hillslope sites (23 ± 9 cm; Figure 5). The Slope Break grid, which sits in the hillslope zone but near the transition from hillslope to riparian, had an intermediate total peat thickness (30 ± 8 cm). The peat thicknesses observed in most riparian sites are underestimates because frozen ground was reached before reaching the bottom of the catotelm; thus, we expect the actual total peat thickness to be larger than what is reported here. The overall increase in peat thickness observed between the hillslope and riparian zone was driven mainly by increases in the catotelm rather than in the acrotelm (Figure 5). A mean acrotelm thickness of 17 cm was observed across both zones; the mean catotelm thickness was significantly larger in riparian settings (33 vs. 8 cm, respectively). We assumed that the riparian sites without thawed loess (i.e., the thaw depth was always above the loess) were composed entirely of peat, and therefore, those data were excluded from further stratigraphic analysis.

The ranges in peat thickness within hillslope sites are caused by the presence and scale of microtopographic features. Microtopographic features are approximately the same size in both hillslope and riparian grids (7.0 and 6.5 cm, respectively; Figure 6); however, within hillslope grids, the stratigraphy underneath local highs differs significantly from that under local lows. 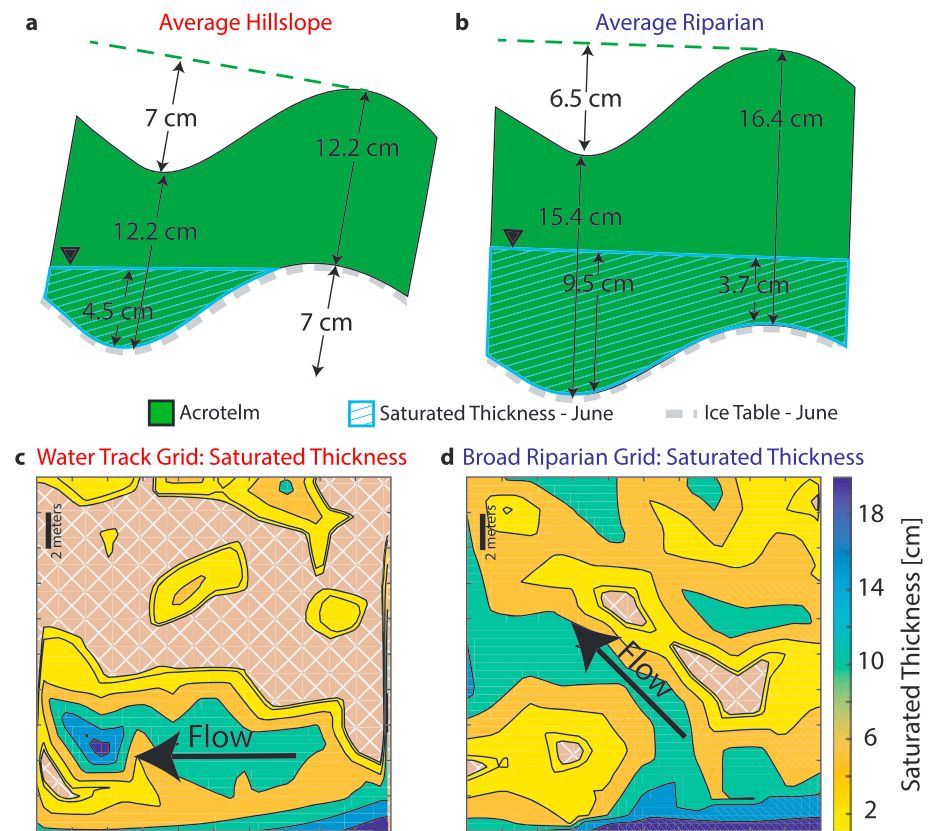This difference arises mainly from changes in acrotelm thickness; local highs have acrotelm thicknesses approximately 1.7 times larger than local lows (Figure 6), while catotelm thicknesses are approximately equal (11.3 cm underneath local highs vs. 11.2 cm underneath local lows). This results in slightly thinner total peat columns underneath microtopographic lows than highs. This relationship is somewhat stronger in water tracks; acrotelm thicknesses within water tracks is less than one third of that outside water tracks (7.0 vs. 20.3 cm, respectively), and catotelm thickness within and outside of water tracks is approximately equal.

In the riparian zone, the mean peat thickness underneath local highs (35.5 cm) was observed to be slightly thinner than the mean peat thickness underneath local lows (40.8 cm); however, these differences were not statistically significant ($p = 0.4$). Despite the lack of statistical significance, there is evidence that microtopography influences total peat thickness; we observed a strong correlation between grid microtopography feature size and peat thickness ($R^2 = 0.98$). Although cryoturbation has been reported in the watershed we studied and in other similar landscapes (Bockheim, 2007; Michaelson et al., 1996), no samples in which the acrotelm-catotelm-loess stratigraphy was interrupted or reversed by freeze-thaw or any other process were encountered.

4.3. Saturated Thickness and Ice and Water Table Depths

As described above, quantifying the thickness of the saturated zone (b) requires identifying the time-varying depths of both the upper boundary (the water table) and the lower boundary (the ice table as determined by thaw depth). The overall findings from the Early and Late Season measurements of those boundaries confirm that aquifer saturated zones are thin, disconnected, and at shallow depths in the soil column in the Early Season, and they are significantly thicker, connected, and deeper in the soil column in August

Figure 6. Schematic representations of microtopography size and land surface slope and their influence on stratigraphy, saturated thickness, and thaw in the Early Season. (a) Average of measurements in the three hillslope grids; (b) average of measurements in the three riparian zone grids. Observed saturated thicknesses in the (c) Water Track grid on the hillslope and the (d) Broad Riparian grid in the riparian area. Black arrows represent the general groundwater flow direction in each grid. Brown hatched pattern represents completely unsaturated soil.

(Figure 5 and Table 2). The findings also show that the Early Season saturated zone is significantly thicker in the riparian area than on the hillslope (Figure 5 and Table 2) and that intergrid microtopography causes the vertical position of b to shift substantially across very short distances.

4.3.1. Hillslope Saturated Thicknesses, Thaw Depths, and Water Table Depths

The early season saturated zone in the hillslope was essentially nonexistent, with pockets of saturation surrounded by mostly "dry" soil (Figure 6c). Among all sites, the mean b was approximately 1 cm; however, 69% of those sites were dry, meaning that the thaw and water table were at the same depth. Among the sites that were not dry, the mean b was approximately 5 cm, with a maximum observed b of 13 cm occurring within the water track portion of the Water Track grid (Figure 6). The vertical position of the saturated zone was very near the surface; the mean thaw depth had only reached 12 cm, and the mean observed water table depth was only 7 cm below the land surface elevation. Local highs were more likely to be dry than local lows (76% vs. 61% of sites, respectively); this is consistent with other findings in the literature (Quinton et al., 2000). However, there was no observed difference in the thaw depth between the highs and lows (11 cm underneath both highs and lows). Because the thaw depth was so shallow, all the saturation in June occurred within the acrotelm.

The saturated pockets within the hillslope became connected by the Late Season because the saturated zone expanded and deepened substantially (Figure 5 and Table 2). The net expansion in the saturated zone occurred because the thaw depth expanded more than the water table deepened; the thaw depth increased by an average of 45 cm across hillslope sites between June and August (Table 2), while the water table only deepened by an average of 10 cm (Table 2). Expansion in b was not homogeneous across the hillslope, however. The populations of b measured within each grid were statistically different ($p < 0.0001$), with the

average b increasing most in the Water Track grid (to 52 cm), less in the Slope Break grid (to 39 cm), and less still in the Inter-Track grid (to 23 cm). The Water Track grid thawed deeply in the Late Season, and this increased thaw occurred both directly in the water track and in the nearby area. The Late Season average thaw depth within the water track portion of the Water Track grid was 95 cm; the average thaw depth in all other areas of this grid was significantly less (67 cm). However, even the water-track-adjacent portion of the Water Track grid had significantly deeper thaw than any other location within the hillslope zone. Deep thaw in water tracks has been observed previously (McNamara et al., 1999; Rushlow & Godsey, 2017).

Despite grids having significantly different b values, the vertical position of the saturated zone within Late Season hillslope grids occurred consistently within the loess. The average measured water table elevation (21 cm) equaled the mean depth to loess in these sites. No significant difference between the b underneath local highs (36 $\pm$ 16 cm) and local lows (41 $\pm$ 20 cm) was observed.

4.3.2. Riparian Zone Saturated Thicknesses, Thaw Depths, and Water Table Depths

Excluding the water track points within the Water Track grid, the thickest saturated layers were consistently observed in the riparian zone (Figure 5 and Table 2). b in the riparian zone averaged 6.3 cm in June, due mainly to a deeper observed thaw depth in the riparian zone than on the hillslope (15.6 vs. 11.1 cm, respectively). The mean water table depth in the riparian zone was also shallow (9 cm). Unlike in the hillslope, less than 10% of riparian sites measured were dry. However, like in the hillslope, the saturated zone thickness and vertical position ranged substantially due to microtopography. b under local lows was approximately three times larger than b under local highs (9.7 vs. 3.6 cm, respectively), and the percentage of dry sites was much lower (6% vs. 18%, respectively). However, the thaw depths underneath local highs and local lows were approximately equal (15.4 vs. 16.3 cm, respectively). As in the hillslope, all the saturation in the Early Season occurred within acrotelm, as the catotelm and loess had yet to be thawed.

The b in the riparian zone also increased between June and August but not as substantially as hillslope b did. The mean b observed in the riparian zone grew 450%, to 35 cm (Table 2). The net expansion in the saturated zone occurred because the thaw depth expanded more than the water table deepened; the thaw depth expanded by 218%, from 16 to 51 cm, while the water table depth only increased by 67%, from 9 to 15 cm.

The net expansion of the saturated zone was greatest under local topographic highs. Although local lows still exhibited significantly larger b than under local highs (43 vs. 28 cm), the seasonal increase in b was much larger underneath local highs than local lows (560% vs. 302%, respectively). Additionally, a significant disparity in thaw depth arose in the Late Season, with thaw underneath local highs averaging 6 cm less than thaw under local lows (48 vs. 54 cm, respectively). Excluding the Water Track grid, the Late Season data show a progression of increasing b with decreasing land surface slope (Figure 5).

4.4. Transmissivity Calculated From Observed Water Table Elevations

Measurements of K with the position and thickness of the saturated zone were used to calculate T for all grid points. Such calculations show that spatial and temporal variability in active layer T is substantial across very small distances. T ranged greatly because K decreased approximately 5 orders of magnitude within a depth of about 60 cm, and the vertical position of the saturated zone varied significantly within that depth across grids and throughout the season. Because K is laterally consistent across soils of the same type, T could be calculated (equation (2)) using the measured soil contact depths, soil K, water table elevations, and thaw depths from the grids. The integral in equation (2) is a piecewise function; the three components reflect the different K observed in the acrotelm (a function that decreases with depth), catotelm (a function that decreases with depth), and loess (a constant). Based on the linear regressions of K measurements with depth (equation (7)), we determined T to be

$$T = \begin{cases} 19.6e^{-44.1z_a} - 19.6e^{-44.1z_1}, & z < z_a \\ 1.24e^{-0.81z_m} - 1.24e^{-0.81z_a}, & z_a < z < z_m, \\ 10^{-2}(z_2 - z_m), & z > z_m \end{cases} \tag{8}$$

where z_1 is the depth of the water table (m), z_2 is the depth to thaw (m), z_a is the depth to the inflection point in the K-depth curve (established to be 0.15 m, Figure 4), z_m is the depth to the catotelm base (if observed; m), and T is expressed in square meters per day. In instances where the catotelm base was not observed, $z_m = z_2$, and the piecewise equation is limited to only the first two items.
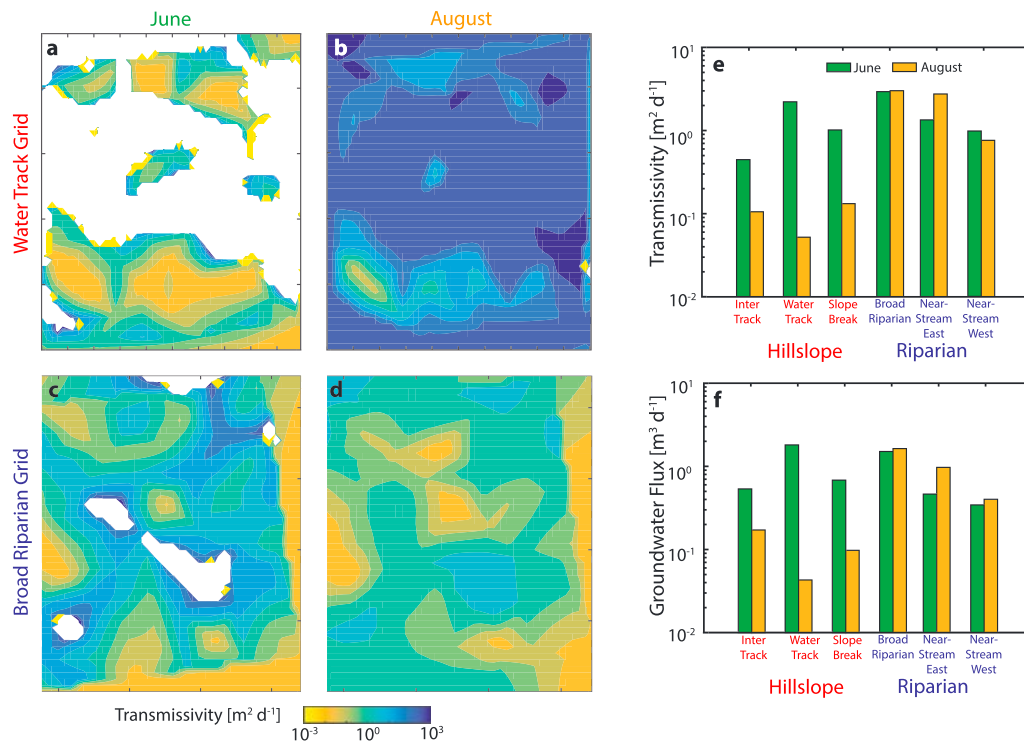
Figure 7. Spatial patterns and temporal snapshots of T and groundwater flow within the study grids. Upper panels show the calculated transmissivities of (a) the Water Track grid in June, (b) the Water Track grid in August, (c) the Broad Riparian grid in June, and (d) the Broad Riparian grid in August. (e) Mean T of each grid in June (green bar) and August (orange bar); (f) total groundwater flow leaving each grid through the 20-m downslope boundary in June (green bar) and August (orange bar).

The riparian zone was consistently more transmissive than the hillslope (Figure 7e and Table 2). In June, the mean hillslope T was 1.17 m^2/day, and the riparian T was significantly larger (2.13 m^2/day). This difference widened in August, when riparian T increased slightly to 2.9 m^2/day, while hillslope T decreased over an order of magnitude to 0.10 m^2/day. The factors that limited T in the hillslope changed between June and August; in June, the average hillslope T was low largely because many locations were dry and thus had a $T = 0$. The average T among only saturated hillslope sites was 1.95 m^2/day, which is comparable to the average T in the riparian sites. In August, hillslope T was not influenced by unsaturated sites, because saturation was ubiquitous across all grids. Hillslope T was low in the Late Season because 96% of the saturation that occurred was in the low-permeability loess. The low K of this soil overwhelmed the increases in b observed, causing the steep seasonal drop in T.

We did not observe a decline in riparian zone T between Early Season and Late Season. Rather, increases in b drove slight increases in T, from 2.13 to 2.9 m^2/day. Increases in b were not overwhelmed by a K decrease because most riparian sites lack a thawed, low-permeability loess layer and because the seasonal thickening of the saturated zone was not accompanied by substantial deepening. The water table depth measured in June across riparian sites (7.6 cm) only fell 4 cm in August (11.7 cm); such shallow saturation ensured that higher-permeability soils were incorporated in the aquifer, keeping the T high.

Microtopographic features caused intergrid T variability to span 5 orders of magnitude (Figures 7a–7d). Variability in T was most prominent in the Early Season because local highs were either unsaturated or minimally saturated. For example, the average Early Season riparian zone T in a local high was an order of magnitude lower than T in a local low (0.36 vs. 3.21 m^2/day, respectively); in the hillslope, the difference was nearly 2 orders of magnitude (0.07 m^2/day in local highs vs. 2.24 m^2/day in local lows). In the Late Season, saturation occurred underneath both local highs and lows, so the disparity between T underneath local highs and local lows shrank significantly (Figure 8). The T in local highs tripled in the riparian zone, to 1.10 m^2/day, while the T in local lows remained constant (3.30 m^2/day). Intergrid T variability
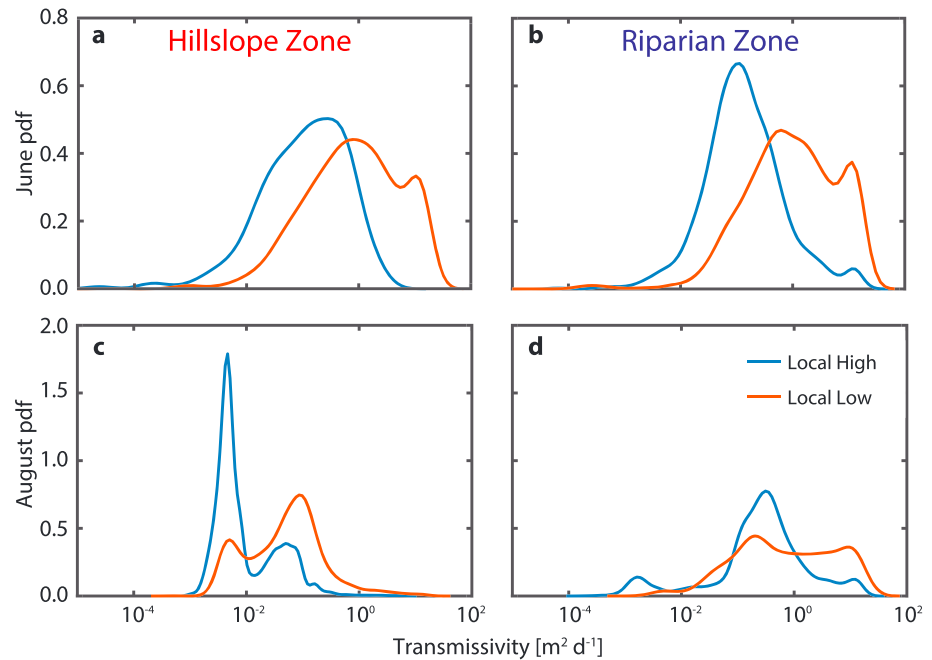
Figure 8. Probability density of calculated T in local highs (blue lines) and local lows (red lines). (a) and (b) show calculated values based on June observations; (c) and (d) show calculated values based on August observations. Left-hand column represents all data points in the hillslope zone; right-hand column represents all data points in the riparian zone.

remained substantial throughout the Late Season in the hillslope. The difference between T in local highs and local lows decreased (0.03 m^2/day in local highs vs. 0.16 m^2/day in local lows); however, even in the Late Season, the difference between T in local highs and local lows was significant because both b and the saturated zone position varied largely between such microtopographic features.

4.5. Measured Groundwater Head Gradients and Calculated Groundwater Flows Based on Early Season and Late Season Scenarios

The measured water table elevations produced a planar surface whose slope mimicked that of the regional topographic gradient (Table 2). Hydraulic head gradients within the riparian zone ranged between 1.5% and 3.9%. Hydraulic head gradients in the hillslope ranged between 5.5% and 11.8%.

The measured hydraulic head gradients and the $K(z)$ function computed above (equation (7)) were used as inputs to 3-D groundwater flow calculations in conjunction with the Early Season and Late Season water table and thaw depth measurements (Figure 9). Each groundwater flow calculation in this study represents the flow through a 20-m-long strip of soil perpendicular to the mean slope, reflecting the dimensions of the study grids (Figure 3). These calculations showed that hillslope groundwater flows are potentially largest in the Early Season and can diminish substantially as the season progresses (Figure 7f and Table 2) but is dependent on rainfall patterns. Groundwater flows in low-gradient riparian zone sites are not expected to change much throughout the entire season (Figure 7f and Table 2).

No strong correlation was observed between the hydraulic head gradient and calculated groundwater flows (Table 2). The highest-gradient grid, the Inter-Track, had the least groundwater flow in both June and August. The lowest-gradient grid, the Near-Stream East (2.7% gradient), yielded the third highest groundwater flow under these June conditions and the second highest flow under these August conditions (Figure 7f).

A strong correlation was observed, however, between T and groundwater flow ($R^2 = 0.7$). In June, when T is high across all grids in both landscape types, the groundwater flow across all grids is high as well (Figure 7). Correspondingly, in August, when T decreases significantly in the hillslope but remains constant in the riparian zone, groundwater flows follow the same pattern. The mean flow from hillslope grids decreased 2
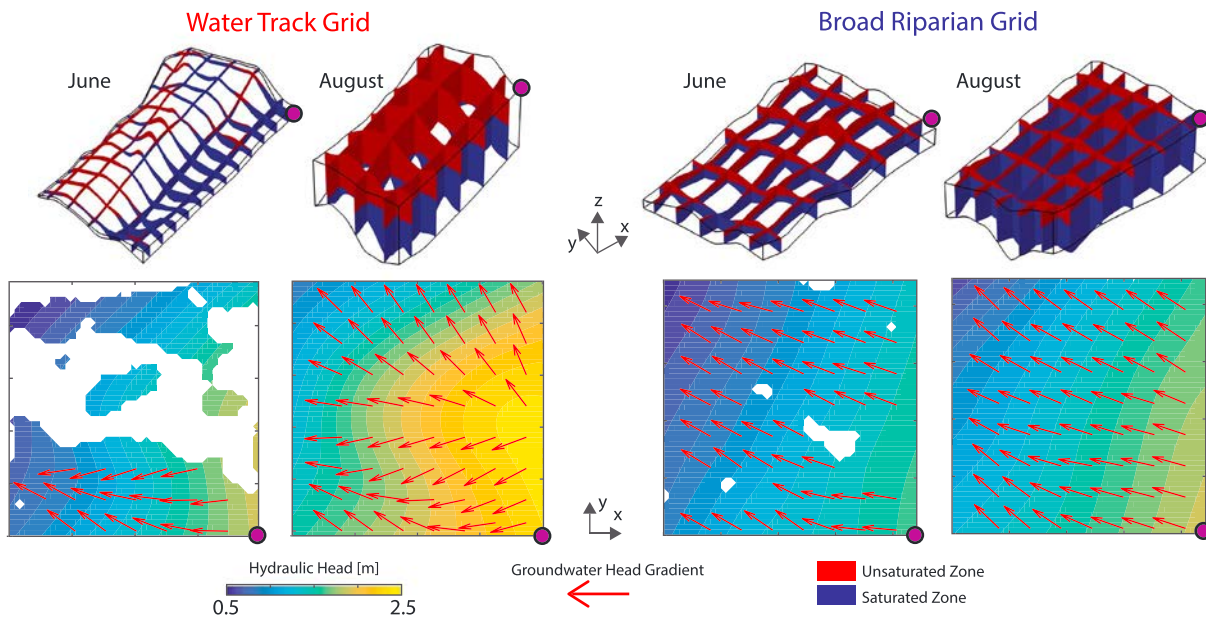
Figure 9. 3-D saturated groundwater flow model results. Top row shows the location of the water table within the domain; bottom row shows the plan view groundwater hydraulic head distribution (contours) and gradients (red arrows). White gaps in the contour fields represent completely dry locations. Purple circles in the corner of the 3-D grids correspond to the same purple circles on the 2-D fields.

orders of magnitude to 0.075 m³/day. However, in the riparian grids, where T remains relatively constant throughout the season, groundwater flows remained constant or increased slightly.

4.6. Sensitivity of Transmissivity and Groundwater Flow to Water Table Location

Both T and groundwater flow were dominated by the highly permeable acrotelm, with the catotelm contributing small flows and the loess providing negligible flow (Figure 10). The T of the upper 15 cm of soil is 10 times larger than the T of remaining riparian zone catotelm (11.4 vs. 1.1 m²/day, respectively) and 12 times larger than that in the hillslope catotelm and mineral soil (11.4 vs. 0.94 m²/day, respectively).

High acrotelm T promotes high groundwater flows. A saturated acrotelm can yield approximately 92% of the total flow from a completely thawed column in the hillslope and 91% of the total flow from a completely thawed column in the riparian area (12.1 and 5.1 m³/day, respectively). Groundwater flows from the high-gradient hillslope acrotelm are more than twice as large as those in the low-gradient riparian zone (Figure 10).

The commonly accepted conceptual structure of peat states that acrotelm generally sits above the long-term mean water table, and catotelm is below (Morris et al., 2011). The water table observations also show that the acrotelm was rarely fully saturated during our data collection periods. While the acrotelm could be a regular component of the active layer saturated zone during rain events, excluding it from transmissivity calculation by considering a column of peat saturated from the long-term water table average (i.e., the acrotelm-catotelm boundary) to the August thaw depth shows that near-surface flow still overwhelms deeper flow. For example, in the hillslope, the T of the approximately 10-cm-thick catotelm layer exceeds the T of the entire loess by 30 times (0.9 vs. 0.03 m²/day, respectively), and the catotelm generates 98% of the total flow (1.04 vs. 0.03 m³/day). A similar but more muted relationship is observed in the riparian zone, despite the absence of loess. Low K at depth causes the T of the upper 10 cm of catotelm (15- to 25-cm depth) to be approximately 4.8 times larger than T in the remaining thickness of the column (from 25-cm depth to the bottom of the active layer thickness of approximately 51 cm). The disparity in T with depth causes 83% of the total column flow to be generated within the upper 10 cm of the catotelm (0.52 vs. 0.08 m³/day). The steeper gradients of the hillslope still cause flow from these zones to be approximately twice the flow from the riparian zone at this depth at the time of our measurements.
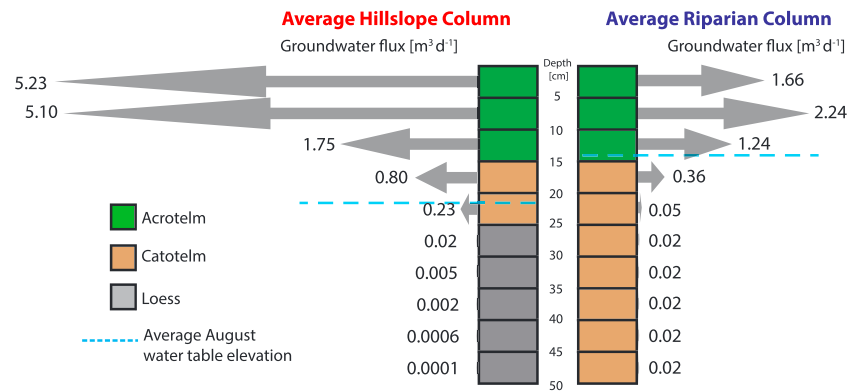
Figure 10. Average groundwater flow rate for individual 5-cm slices of a column of (left) the average hillslope active layer and (right) the average riparian active layer. Groundwater flows are based on a column of soil with a length of 20 m, a width of 20 m, a depth of 5 cm, and porosity determined from observations (see Figure 4).

5. Discussion

This study quantitatively shows that the thickening and deepening of the active layer does not always exert an appreciable control on groundwater flows. At our study sites, the impact that active layer thickening has on groundwater flows depends most on the position (depth) of the saturated thickness and the properties of the active layer soil column (such as hydraulic conductivity), which correlates strongly with landscape type. While this has been suggested before (i.e., Wright et al., 2009), our analysis provides a quantitative assessment of this impact and shows it to be true at different times (early versus late season) and in different landscape zones (hillslopes versus riparian zones). Given the soil profiles observed at the study site, active layers that contain near-surface saturated zones will transmit much more groundwater than active layers with deep saturated zones, irrespective of the landscape type. The sensitivity analysis for water table location showed that the upper 10 cm of active layer soil, within the acrotelm, can transmit over 600% more water than the rest of the thawed column, despite being one fifth the size. The position of the saturated zone dominates groundwater flows because the saturated zone is imposed on a K profile that decays exponentially with depth, which strongly decreases both T and groundwater flow. The observed decrease in K with depth agrees well with patterns observed in continuous permafrost environments (Hinzman et al., 1991; Quinton et al., 2000), boreal environments (Ebel et al., 2019; Quinton et al., 2004; Quinton et al., 2008), and other peat-dominated environments lacking permafrost (Beckwith et al., 2003). However, the results here reveal a steeper decay over a shorter depth interval than other studies in similar settings.

The hillslopes and riparian zones within the Imnavait Creek watershed transport equal volumes of groundwater in the Early Season, but riparian zones are substantially better at transporting groundwater than hillslopes in the Late Season. This is because landscape zone (i.e., hillslope zone and riparian zone) dictated the position of the saturated layer within the soil column, which correspondingly determined groundwater flows. We observed the saturated zone in riparian areas to be near the surface across both the Early and Late Season, whereas the hillslope saturated zone deepened significantly in the Late Season. The average riparian saturated zone position dropped only 6 cm across the season (from 9 ± 4 to 15 ± 7 cm), while in the hillslope, the water table dropped twice as much (from 9 ± 4 to 21 ± 7 cm). Even in the Late Season, therefore, 50% of the sites measured in the riparian zone have a saturated zone that sits in the highly permeable acrotelm. In contrast, only 15% of the sites measured on the hillslope have a saturated zone in the acrotelm, and thus, much more of the flow occurs in the less permeable, deeper soils. The continuous position of a saturated zone in the near surface provides a mechanistic explanation for why riparian groundwater flows remained constant across the season, while hillslope groundwater flows decreased by an order of magnitude.

Our data show that seasonal thaw may result in a deepening of the saturated zone in both Imnavait Creek hillslope and riparian zone settings. Our data also show that thaw almost always causes a thickening of the saturated zone in our study area. Thaw provides the potential for shallow groundwater to migrate downward but only if there is available void space within those deeper, thawing soils. Thaw into an already saturated loess column would not cause any downward migration of shallow groundwater; however, that thaw

would substantially increase saturated zone thickness (*b*). Thawing into deeper, unsaturated soils, which typically have lower porosity than soils near the surface (Figure 4), could also increase *b* incrementally, because the same volume of water occupies a larger volume of lower porosity soil. While we do observe a pronounced downward shift in the hillslope saturated zone between seasons, it is unlikely that such shifting is due to the overall downward migration of shallow groundwater. The *K* of deeper soils is quite low, which limits the ability for these soil layers to drain within a season. Saturation is likely a persistent condition in these deep soils, and our observed water table deepening is more likely due to the outward, lateral (downslope) draining of much higher-*K* organic soil coupled with simultaneous thawing into saturated loess soil.

These results capture two temporal snapshots of active layer saturated zones, and it has been shown that in seasonally thawed active layers, precipitation and drainage can cause the water table to fluctuate substantially in short time periods (Quinton & Gray, 2003; Roulet et al., 1993; Woo & Steer, 1983; Wright et al., 2009). This study does not attempt to model the effect of such fluctuations on groundwater flow, but multiple lines of evidence suggest that the spatial and temporal patterns we observed in saturated zone thickness and position are representative of other permafrost environments. For example, in the Early Season, the saturated zone will exclusively occur in the acrotelm in both hillslope and riparian landscape zones, because it is the only soil type that is thawed at that time. In the Late Season, it is likely that frequent, summer precipitation events could cause the acrotelm in the riparian zone to partially or completely saturate and to influence hillslope saturation conditions or groundwater export. One such event occurred during our Late Season measurements. This event, on 7 August 2016, led to approximately 4 mm of rainfall at Toolik Field Station, which falls just above the average amount of a daily rainfall event calculated from all rain events from 2011 to 2017 (3.56 mm/day, Toolik Field Station, Environmental Data Center, https://toolik.alaska.edu/edc/). The precipitation that fell on the watershed that day elevated the riparian zone water table into the acrotelm, saturating the soil nearly to the surface and increasing groundwater flows. Precipitation failed to elevate the water levels on the hillslope over the time scales that we were able to measure; rather, the high land-surface slopes on the hillslope likely led to rapid downslope transport of this precipitation into the riparian zone. This connectivity between hillslope and riparian zone has been demonstrated in the past (Stieglitz et al., 2003). The hillslope provides a source of water necessary to maintain riparian zone late-season *b* that can include the highly permeable acrotelm, and the low slope of the riparian zone prevents it from draining out rapidly. Given that the rain event magnitude we observed was slightly above the mean rain event magnitude, we could expect that flows through the riparian zone acrotelm are a common occurrence; this also supports our conclusion that riparian zones are substantially better at transmitting water in the Late Season than are hillslopes.

We also observe different results between the Imnavait Creek hillslope and riparian zones in the effect of the continually deepening depth of thaw (ice table) on both *b* and groundwater flow. These different results occur because of the distinct stratigraphy between the zones. In the riparian zone, only a two-layer soil stratigraphy was observed, where highly permeable acrotelm overlaid less permeable catotelm. Only in the hillslope does extremely low-*K* loess exist within the depth that is thawed, and the Late Season *b* in the hillslope deepens into that loess, while the Late Season *b* in the riparian zone remains entirely in peat. The small *K* of hillslope loess leads to an approximate order of magnitude decrease in flow compared to catotelm peat at the same depth in the riparian zone (Figure 10). The presence of this loess, in conjunction with a lack of acrotelm flow, explains why *T* and groundwater flow in the hillslope are significantly smaller than in the riparian zone in the Late Season, despite similar increases in *b* from the Early Season conditions (Figure 6). The widespread distribution of loess across the landscape (Walker & Everett, 1991), combined with its distinctly different hydraulic properties from catotelm, suggests that loess may provide a strong limitation on deep groundwater flow rates across the region and highlights the importance of identifying the loess-catotelm contact to build a complete understanding of groundwater flows in the region.

The ice table depth does not substantially influence groundwater flows in the Late Season in either landscape zone due to low-permeability soils at depth, but the ice table depth does exert a strong control on Early Season groundwater flows by causing subsurface flow barriers that withhold groundwater within microtopographic features. Microtopographic surface features drive spatial variability in the thaw depth, which creates pockets of saturation disconnected from flowpaths, temporarily trapping water in place (Figures 6 and 9). Water in these pockets is unable to move because it is surrounded by dry local highs. Such microtopographic withholding is landscape-specific, with more withholding occurring in the

hillslope zone than in the riparian zone. The thaw depth difference under local highs between the two landscape zones was minimal; however, in the hillslope, the water table depths were, on average, 2 cm below the ice table of a local high (Figure 6). Groundwater is therefore commonly retained within local lows on the hillslope. While thaw depth between local highs and lows in the riparian zone varied, the water table still sat above the thaw depth in most locations, leading to fewer isolated pockets.

Microtopography-induced withholding of groundwater has been observed at local scales in permafrost settings (Quinton et al., 2000) and at basin scales where an uneven bedrock bottom can cause groundwater to be similarly withheld behind bedrock dams (Tromp-van Meerveld & McDonnell, 2006) and has strong implications for groundwater age. Water in a local low that exists deeper than a nearby ice dam is effectively disconnected from the free-flowing surface layer unless there is a substantial upward component of deeper groundwater flow directing it toward the free-flowing surface layer. Because generation of such an upward component is difficult with underlying permafrost, the deeper, trapped water is therefore only free to flow once the ice barrier thaws. Given that we observed microtopography-driven spatial variability in the thaw depth to increase over the summer season, there are always depths at which water underneath local lows is trapped by ice barriers underneath local highs. While this water cannot flow laterally, it is possible that future warming or mechanical processes such as frost wedging could alter ice dams (Liljedahl & Hinzman, 2012; Zhang, 2014) and potentially allow the trapped water to escape. This could lead to a threshold influx of unexpectedly old groundwater into connected flow pathways.

6. Implications

Future climate warming will increase the active layer thickness of continuous permafrost environments (Lawrence et al., 2011) such as the Imnavait Creek Watershed. There is widespread debate within the literature on the impact of this active layer thickening on future suprapermafrost groundwater flows. Many previous studies suggest that thickening of the active layer may increase groundwater flows (Evans & Ge, 2017; Kurylyk et al., 2016; Walvoord & Kurylyk, 2016; Walvoord & Striegl, 2007), while others suggest that soil compaction could decrease baseflows (Koch et al., 2014). Our results suggest that the impact of active layer thickening, for watersheds similar to Imnavait Creek, will depend on location in the watershed. For example, we show that groundwater increases due to active layer thickening are negligible in loess-dominated locations such as the hillslope zone and moderate in catotelm-dominated locations such as the riparian zone. However, these changes are dwarfed by precipitation-driven groundwater flow increases, because precipitation introduces new water at the top of the soil column where hydraulic conductivities are the highest. It has been shown that the streams in such basins are supplied nearly entirely by groundwater flowing through or exchanging with this high-K zone (Neilson et al., 2018). It is therefore necessary to know how K changes with depth across space, and how precipitation will change in the future, to predict the impact of climate change on groundwater flow.

A thicker, thawed soil column has a relatively large effect on groundwater flows down through catotelm, but an insignificant effect if the soils are loess. Results from our Variable Water Table sensitivity analysis show current groundwater contributions from loess in the hillslope to be ~0.029 m^3/day (across our 20-m-wide downslope grid boundary); assuming loess hydraulic properties are constant with depth, expanding the thawed loess column by 300% results in a flow of 0.09 m^3/day and increase of ~0.06 m^3/day. Comparatively, in the riparian area, a 300% thicker catotelm column would increase groundwater flows approximately 10 times more (~0.6 m^3/day), from 0.49 to 1.13 m^3/day, assuming a decrease in K with depth extrapolated from our measurements (Figure 4 and equation (8)). It is therefore necessary to identify the location and depth of the contact between loess and peat soil in watersheds to better predict future groundwater contributions as thaw increases. In areas with relatively thin peat layers underlain by loess, it is unlikely that groundwater flows will be affected by active layer expansion; however, in cases of substantial active layer expansion coupled with minimal water table migration, groundwater flows can increase significantly (Ge et al., 2011). In areas with thick peat sequences, substantial flow increases are possible simply through active layer deepening, depending on precipitation amounts.

The decrease in K with depth currently provides a limitation to groundwater flows that will likely continue into the foreseeable future. Loess soils provide a much stronger limitation than catotelm soils because K in the deepest, most compressed peat was still 2 orders of magnitude greater than K in the most permeable

loess. This pattern likely continues beyond the depths we measured because peat compaction at depth, due both to the weight of overbearing soil and the microbial degradation of the organic material, can extend tens of meters deep (e.g., Beckwith et al., 2003). If we extrapolate the increase in compaction (i.e., decrease in K) with depth in the riparian soils, the K of peat would exceed that of loess until a depth of approximately 5.75 m. It is unlikely that such deep soils will be thawed soon. Simulations of active layer dynamics in continuous permafrost near Utqiagvik, Alaska, predict that rising temperatures could drive an approximately 300% expansion in active layer thickness in the next 100 years (Atchley et al., 2015). This thaw expansion would result in future active layer thicknesses that range between 1.3 and 2.2 m if applied to the current thaw depths measured in our grids—depths well short of the 5.75 m necessary for peat K to equal loess K.

7. Conclusions

This study shows that for a watershed in the Foothills of the North Slope of Alaska, active layer suprapermafrost groundwater flows are dominantly controlled by thin, near-surface saturated zones, with saturated zones at greater depth playing a minimal role. Therefore, changes in water table depth at the top of the soil column exert a stronger control on groundwater fluxes than do changes in ice table depth at the bottom. Water table fluctuations near the land surface translate into active-layer aquifer K values that vary by multiple orders of magnitude because the observed decrease in K with depth declines most sharply in the shallow acrotelm and catotelm soils that comprise the top two layers. Conversely, ice table fluctuations occur at the base of the aquifer where the decrease in K with depth declines less rapidly in riparian zones or within constant but low-K loess soils in hillslopes. Therefore, changes in thaw depth have less of an impact on groundwater flows than do changes to the water table depth, despite causing potentially significant changes to the position or the thickness of the saturated zone. In other words, our observations illustrate that given the soil profiles observed within the study watershed, where peat overlying glacial loess is the predominant near-surface stratigraphy, the effect of decreasing K due to saturated zone deepening dominates over increasing b due to thaw. In such environments, barring substantial changes to the subsurface stratigraphy, this pattern is likely to continue as the climate warms and suprapermafrost aquifers expand vertically with thawing.

Significant spatial patterns in both the position of the active layer saturated zone and the shape of the profile of decreasing K with depth were observed, and such patterns caused groundwater flows across the watershed to vary between but not within the riparian or hillslope zones. Within hillslope soils, a low-K loess layer at approximately 25-cm depth caused groundwater flows from below that depth to be insignificant in comparison to flows from equal depths within the riparian zone, which lacked this loess layer. Steep hillslopes therefore only transport substantial quantities of groundwater for brief periods because high-K surface soils rapidly drain. Shallower-slope riparian areas provide both low enough gradients that groundwater can remain longer, keeping water tables high, and contain thick catotelm soils whose intermediate K allows for persistent flow across the thawed seasons.

Groundwater flows were also strongly influenced by microtopography. Microtopography creates significant spatial variability in b and T at the meter scale by retaining groundwater behind ice dams. This phenomenon happened more readily in hillslopes than in riparian zones. Microtopographic retention may exert a substantial effect on the age distribution of groundwater in the basin.

The insights from the study watershed on the effects of stratigraphy, thawing, and microtopography and macrotopography on suprapermafrost groundwater flow suggest that such factors are important to consider not only for quantifying groundwater's role and contributions to present hydrologic and solute budgets but also for predicting the potential expansion and impacts of suprapermafrost groundwater in the future.

References

Atchley, A. L., Painter, S. L., Harp, D. R., Coon, E. T., Wilson, C. J., Liljedahl, A. K., & Romanovsky, V. E. (2015). Using field observations to inform thermal hydrology models of permafrost dynamics with ATS (v0.83). *Geoscientific Model Development*, *8*(9), 2701–2722. https://doi.org/10.5194/gmd-8-2701-2015

Beckwith, C. W., Baird, A. J., & Heathwaite, A. L. (2003). Anisotropy and depth-related heterogeneity of hydraulic conductivity in a bog peat. I: Laboratory measurements. *Hydrological Processes*, *17*(1), 89–101. https://doi.org/10.1002/hyp.1116

Blaen, P. J. (2013). Water source dynamics of high Arctic river basins. *Hydrological Processes*, *28*(10), 3521–3538. https://doi.org/10.1002/hyp.9891

Bockheim, J. G. (2007). Importance of cryoturbation in redistributing organic carbon in permafrost-affected soils. *Soil Science Society of America Journal*, *71*(4), 1335. https://doi.org/10.2136/sssaj2006.0414N

Bouwer, H., & Rice, R. C. (1976). A slug test for determining hydraulic conductivity of unconfined aquifers with completely or partially penetrating wells. *Water Resources Research*, *12*(3), 423–428. https://doi.org/10.1029/WR012i003p00423

Cardenas, M. B. (2010). Lessons from and assessment of Boussinesq aquifer modeling of a large fluvial island in a dam-regulated river. *Advances in Water Resources*, *33*(11), 1359–1366. https://doi.org/10.1016/j.advwatres.2010.03.015

Carman, P. C. (1956). *Flow of gases through porous media*. New York: Academic Press.

Detterman, R. L., Bowsher, A. L., & Dutro, J. T. (1958). Glaciation on the Arctic Slope of the Brooks Range, Northern Alaska. *Arctic*, *11*(1), 43–61. https://doi.org/10.14430/arctic3732

Ebel, B. A., Koch, J. C., & Walvoord, M. A. (2019). Soil physical, hydraulic, and thermal properties in Interior Alaska, USA: Implications for hydrologic response to thawing permafrost conditions. *Water Resources Research*, *55*, 4427–4447. https://doi.org/10.1029/2018WR023673

Evans, S., & Ge, S. (2017). Contrasting hydrogeologic responses to warming in permafrost and seasonally frozen ground hillslopes. *Geophysical Research Letters*, *44*, 1803–1813. https://doi.org/10.1002/2016GL072009

Frampton, A., Painter, S., Lyon, S. W., & Destouni, G. (2011). Non-isothermal, three-phase simulations of near-surface flows in a model permafrost system under seasonal variability and climate change. *Journal of Hydrology*, *403*(3–4), 352–359. https://doi.org/10.1016/j.jhydrol.2011.04.010

Freeze, R. A., & Cherry, J. A. (1979). *Groundwater*. Englewood Cliffs, NJ: Prentice-Hall.

Frey, K. E., & McClelland, J. W. (2009). Impacts of permafrost degradation on Arctic river biogeochemistry. *Hydrological Processes*, *23*(1), 169–182. https://doi.org/10.1002/hyp.7196

Ge, S., McKenzie, J., Voss, C., & Wu, Q. (2011). Exchange of groundwater and surface-water mediated by permafrost response to seasonal and long term air temperature variation. *Geophysical Research Letters*, *38*, L14402. https://doi.org/10.1029/2011GL047911

Hamilton, T. D. (1982). A late Pleistocene glacial chronology for the southern Brooks Range: Stratigraphic record and regional significance. *GSA Bulletin*, *93*(8), 700–716. https://doi.org/10.1130/0016-7606(1982)93<700:ALPGCF>2.0.CO;2

Hinkel, K. M., & Nelson, F. E. (2003). Spatial and temporal patterns of active layer thickness at Circumpolar Active Layer Monitoring (CALM) sites in northern Alaska, 1995–2000. *Journal of Geophysical Research*, *108*(D2), 8168. https://doi.org/10.1029/2001JD000927

Hinzman, L. D., Kane, D. L., Gieck, R. E., & Everett, K. R. (1991). Hydrologic and thermal properties of the active layer in the Alaskan Arctic. *Cold Regions Science and Technology*, *19*(2), 95–110. https://doi.org/10.1016/0165-232X(91)90001-W

Hobbie, J., & Kling, G. (2014). *Alaska's changing Arctic: Ecological consequences for tundra, streams, and lakes (1 edition)*. Oxford; New York: Oxford University Press.

Holden, J., & Burt, T. P. (2003). Hydrological studies on blanket peat: The significance of the acrotelm-catotelm model. *Journal of Ecology*, *91*(1), 86–102. https://doi.org/10.1046/j.1365-2745.2003.00748.x

Koch, J., Kikuchi, C., Wickland, K., & Schuster, P. (2014). Runoff sources and flow paths in a partially burned, upland boreal catchment underlain by permafrost. *Water Resources Research*, *50*, 8141–8158. https://doi.org/10.1002/2014WR015586

Kurylyk, B., Hayashi, M., Quinton, W., McKenzie, J., & Voss, C. (2016). Influence of vertical and lateral heat transfer on permafrost thaw, peatland landscape transition, and groundwater flow. *Water Resources Research*, *52*, 1286–1305. https://doi.org/10.1002/2015WR018057

Lawrence, D. M., Slater, A. G., & Swenson, S. C. (2011). Simulation of present-day and future permafrost and seasonally frozen ground conditions in CCSM4. *Journal of Climate*, *25*(7), 2207–2225. https://doi.org/10.1175/JCLI-D-11-00334.1

Liljedahl, A., & Hinzman, L. (2012). Ice-wedge polygon type controls low-gradient watershed-scale hydrology. In *Tenth International Conference on Permafrost Vol. 1: International Contributions*, (Vol. 1, pp. 231–236). Salekhard, Russia: The Northern Publisher.

Liu, Y., Tong, J., & Li, X. (2005). Analysing the silt particles with the Malvern Mastersizer 2000. *Water Conservancy Science and Technology and Economy*, *11*(6), 329–331.

McNamara, J. P., Kane, D. L., & Hinzman, L. D. (1997). Hydrograph separations in an Arctic watershed using mixing model and graphical techniques. *Water Resources Research*, *33*(7), 1707–1719. https://doi.org/10.1029/97WR01033

McNamara, J. P., Kane, D. L., & Hinzman, L. D. (1999). An analysis of an Arctic channel network using a digital elevation model. *Geomorphology*, *29*(3-4), 339–353. https://doi.org/10.1016/S0169-555X(99)00017-3

Merck, M. F., Neilson, B. T., Cory, R. M., & Kling, G. W. (2012). Variability of in-stream and riparian storage in a beaded Arctic stream. *Hydrological Processes*, *26*(19), 2938–2950. https://doi.org/10.1002/hyp.8323

Michaelson, G. J., Ping, C. L., & Kimble, J. M. (1996). Carbon storage and distribution in tundra soils of Arctic Alaska, U.S.A. *Arctic and Alpine Research*, *28*(4), 414–424. https://doi.org/10.2307/1551852

Morris, P. J., Waddington, J. M., Benscoter, B. W., & Turetsky, M. R. (2011). Conceptual frameworks in peatland ecohydrology: Looking beyond the two-layered (acrotelm–catotelm) model. *Ecohydrology*, *4*(1), 1–11. https://doi.org/10.1002/eco.191

Neilson, B. T., Cardenas, M. B., O'Connor, M. T., Rasmussen, M. T., King, T. V., & Kling, G. W. (2018). Groundwater flow and exchange across the land surface explain carbon export patterns in continuous permafrost watersheds. *Geophysical Research Letters*, *45*, 7596–7605. https://doi.org/10.1029/2018GL078140

Nelson, F. E., Shiklomanov, N. I., & Mueller, G. R. (1999). Variability of active-layer thickness at multiple spatial scales, North-Central Alaska, U.S.A. *Arctic, Antarctic, and Alpine Research*, *31*(2), 179–186. https://doi.org/10.2307/1552606

Omernik, J. M., & Griffith, G. E. (2014). Ecoregions of the Conterminous United States: Evolution of a hierarchical spatial framework. *Environmental Management*, *54*(6), 1249–1266. https://doi.org/10.1007/s00267-014-0364-1

Osterkamp, T. E., & Payne, M. W. (1981). Estimates of permafrost thickness from well logs in northern Alaska. *Cold Regions Science and Technology*, *5*(1), 13–27. https://doi.org/10.1016/0165-232X(81)90037-9

Ping, C.-L., Michaelson, G. J., Jorgenson, M. T., Kimble, J. M., Epstein, H., Romanovsky, V. E., & Walker, D. A. (2008). High stocks of soil organic carbon in the North American Arctic region. *Nature Geoscience*, *1*(9), 615–619. https://doi.org/10.1038/ngeo284

Pomeroy, J. W., Gray, D. M., Brown, T., Hedstrom, N. R., Quinton, W. L., Granger, R. J., & Carey, S. K. (2007). The cold regions hydrological model: A platform for basing process representation and model structure on physical evidence. *Hydrological Processes*, *21*(19), 2650–2667. https://doi.org/10.1002/hyp.6787

Quinton, W. L., Carey, S. K., & Goeller, N. T. (2004). Snowmelt runoff from northern alpine tundra hillslopes: Major processes and methods of simulation. *Hydrology and Earth System Sciences*, *8*(5), 877–890. https://doi.org/10.5194/hess-8-877-2004

Quinton, W. L., & Gray, D. M. (2003). Subsurface drainage from organic soils in permafrost terrain: The major factors to be represented in a runoff model. In Proceedings of the Eighth International Conference on Permafrost, Davos, Switzerland, 6pp.

Quinton, W. L., Gray, D. M., & Marsh, P. (2000). Subsurface drainage from hummock-covered hillslopes in the Arctic tundra. *Journal of Hydrology*, *237*(1–2), 113–125. https://doi.org/10.1016/S0022-1694(00)00304-8

Quinton, W. L., Hayashi, M., & Carey, S. K. (2008). Peat hydraulic conductivity in cold regions and its relation to pore size and geometry. *Hydrological Processes*, *22*(15), 2829–2837. https://doi.org/10.1002/hyp.7027

Quinton, W. L., Shirazi, T., Carey, S. K., & Pomeroy, J. W. (2005). Soil water storage and active-layer development in a sub-alpine tundra hillslope, southern Yukon Territory, Canada. *Permafrost and Periglacial Processes*, *16*(4), 369–382. https://doi.org/10.1002/ppp.543

Roulet, N. T., Ash, R., Quinton, W., & Moore, T. (1993). Methane flux from drained northern peatlands: Effect of a persistent water table lowering on flux. *Global Biogeochemical Cycles*, *7*(4), 749–769. https://doi.org/10.1029/93GB01931

Rushlow, C. R., & Godsey, S. E. (2017). Rainfall–runoff responses on Arctic hillslopes underlain by continuous permafrost, North Slope, Alaska, USA. *Hydrological Processes*, *31*(23), 4092–4106. https://doi.org/10.1002/hyp.11294

Schramm, I., Boike, J., Bolton, W. R., & Hinzman, L. D. (2007). Application of TopoFlow, a spatially distributed hydrological model, to the Imnavait Creek watershed, Alaska. *Journal of Geophysical Research*, *112*, G04S46. https://doi.org/10.1029/2006JG000326

Schuh, C., Frampton, A., & Christiansen, H. H. (2017). Soil moisture redistribution and its effect on inter-annual active layer temperature and thickness variations in a dry loess terrace in Adventdalen, Svalbard. *The Cryosphere*, *11*(1), 635–651. https://doi.org/https://doi.org/10.5194/tc-11-635-2017

Smith, S. L., Wolfe, S. A., Riseborough, D. W., & Nixon, F. M. (2009). Active-layer characteristics and summer climatic indices, Mackenzie Valley, Northwest Territories, Canada. *Permafrost and Periglacial Processes*, *20*(2), 201–220. https://doi.org/10.1002/ppp.651

Stieglitz, M., Shaman, J., McNamara, J., Engel, V., Shanley, J., & Kling, G. W. (2003). An approach to understanding hydrologic connectivity on the hillslope and the implications for nutrient transport. *Global Biogeochemical Cycles*, *17*(4), 1105. https://doi.org/10.1029/2003GB002041

Surridge, B. W. J., Baird, A. J., & Heathwaite, A. L. (2005). Evaluating the quality of hydraulic conductivity estimates from piezometer slug tests in peat. *Hydrological Processes*, *19*(6), 1227–1244. https://doi.org/10.1002/hyp.5653

Trexler, J. C., & Travis, J. (1993). Nontraditional regression analyses. *Ecology*, *74*(6), 1629–1637. https://doi.org/10.2307/1939921

Tromp-van Meerveld, H. J., & McDonnell, J. J. (2006). Threshold relations in subsurface stormflow: 2. The fill and spill hypothesis. *Water Resources Research*, *42*, W02411. Retrieved from. https://doi.org/10.1029/2004WR003800/full

van Asselen, S., Stouthamer, E., & van Asch, T. W. J. (2009). Effects of peat compaction on delta evolution: A review on processes, responses, measuring and modeling. *Earth-Science Reviews*, *92*(1–2), 35–51. https://doi.org/10.1016/j.earscirev.2008.11.001

Voytek, E., Rushlow, C., Godsey, S., & Singha, K. (2016). Identifying hydrologic flowpaths on Arctic hillslopes using electrical resistivity and self potential. *Geophysics*, *81*(1), WA225–WA232. https://doi.org/10.1190/geo2015-0172.1

Wahrhaftig, C. (1965). *Physiographic divisions of Alaska*. Washington, DC: US Government Printing Office.

Walker, D. A., & Everett, K. R. (1991). Loess ecosystems of Northern Alaska: Regional gradient and toposequence at Prudhoe Bay. *Ecological Monographs*, *61*(4), 437–464. https://doi.org/10.2307/2937050

Walker, D. A., Jia, G. J., Epstein, H. E., Raynolds, M. K., Chapin, F. S. III, Copass, C., et al. (2003). Vegetation-soil-thaw-depth relationships along a low-Arctic bioclimate gradient, Alaska: Synthesis of information from the ATLAS studies. *Permafrost and Periglacial Processes*, *14*(2), 103–123. https://doi.org/10.1002/ppp.452

Walker, D. A., & Walker, M. D. (1996). Terrain and vegetation of the Imnavait Creek watershed. In *Landscape function and disturbance in Arctic tundra* (pp. 73–108). New York: Springer. Retrieved from https://doi.org/10.1007/978-3-662-01145-4_4

Walvoord, M. A., & Kurylyk, B. L. (2016). Hydrologic impacts of thawing permafrost—A review. *Vadose Zone Journal*, *15*(6). https://doi.org/10.2136/vzj2016.01.0010

Walvoord, M. A., & Striegl, R. G. (2007). Increased groundwater to stream discharge from permafrost thawing in the Yukon River basin: Potential impacts on lateral export of carbon and nitrogen. *Geophysical Research Letters*, *34*, L12402. https://doi.org/10.1029/2007GL030216

Wang, H. F., & Anderson, M. P. (1995). *Introduction to groundwater modeling: Finite difference and finite element methods*. London: Academic Press.

Woo, M. (2012). *Permafrost hydrology*. Berlin Heidelberg: Springer-Verlag. Retrieved from. https://www.springer.com/us/book/9783642234613, https://doi.org/10.1007/978-3-642-23462-0

Woo, M., & Steer, P. (1983). Slope hydrology as influenced by thawing of the active layer, Resolute, N.W.T. *Canadian Journal of Earth Sciences*, *20*(6), 978–986. https://doi.org/10.1139/e83-087

Wright, N., Hayashi, M., & Quinton, W. L. (2009). Spatial and temporal variations in active layer thawing and their implication on runoff generation in peat-covered permafrost terrain. *Water Resources Research*, *45*, W05414. https://doi.org/10.1029/2008WR006880

Zhang, Y. (2014). Thermal-hydro-mechanical model for freezing and thawing of soils. Retrieved from http://deepblue.lib.umich.edu/handle/2027.42/108828